REPORT DOCUMENTATION PAGE

Form Approved OMB NO. 0704-0188

1. REPORT DATE (DD-MM-YYYY)	2. REPORT TYPE	3. DATES COVERED (From - To)
	New Reprint	-

4. TITLE AND SUBTITLE

Influence of Indium Tin Oxide Surface Treatment on Spatially Localized Photocurrent Variations in Bulk Heterojunction Organic Photovoltaic Devices

5a. CONTRACT NUMBER	W911NF-05-1-0177
5b. GRANT NUMBER	
5c. PROGRAM ELEMENT NUMBER	611102
5d. PROJECT NUMBER	
5e. TASK NUMBER	
5f. WORK UNIT NUMBER	

6. AUTHORS

Benjamin J. Leever, Ian P. Murray, Michael F. Durstock, Tobin J. Marks, Mark C. Hersam

7. PERFORMING ORGANIZATION NAMES AND ADDRESSES

Northwestern University Chicago Campus
Office of Sponsored Research
Northwestern University
Evanston, IL 60208 -1110

8. PERFORMING ORGANIZATION REPORT NUMBER

9. SPONSORING/MONITORING AGENCY NAME(S) AND ADDRESS(ES)

U.S. Army Research Office
P.O. Box 12211
Research Triangle Park, NC 27709-2211

10. SPONSOR/MONITOR'S ACRONYM(S)
ARO

11. SPONSOR/MONITOR'S REPORT NUMBER(S)
48138-CH-PCS.19

12. DISTRIBUTION AVAILIBILITY STATEMENT

Approved for public release; distribution is unlimited.

13. SUPPLEMENTARY NOTES

The views, opinions and/or findings contained in this report are those of the author(s) and should not contrued as an official Department of the Army position, policy or decision, unless so designated by other documentation.

14. ABSTRACT

A correlation between anode surface treatment and spatially localized photocurrent variations has been found in bulk heterojunction poly(3-hexylthiophene):[6,6]-phenyl-C-61-butyric acid methyl ester (P3HT:PCBM) organic photovoltaic (OPV) devices. Atomic force photovoltaic microscopy (AFPM) was used to scan arrays of 2 ?m diameter OPV devices with varied indium tin oxide (ITO) surface treatments. The standard deviation of the average photocurrent was found to be 11.4% for devices fabricated on untreated ITO, 8.6% for devices with a

15. SUBJECT TERMS

indium tin oxide, organic photovoltaics, atomic force photovoltaic microscopy

16. SECURITY CLASSIFICATION OF:			17. LIMITATION OF ABSTRACT	15. NUMBER OF PAGES	19a. NAME OF RESPONSIBLE PERSON
a. REPORT	b. ABSTRACT	c. THIS PAGE			Mark Hersam
UU	UU	UU	UU		19b. TELEPHONE NUMBER: 847-491-2696

Report Title

Influence of Indium Tin Oxide Surface Treatment on Spatially Localized Photocurrent Variations in Bulk Heterojunction Organic Photovoltaic Devices

ABSTRACT

A correlation between anode surface treatment and spatially localized photocurrent variations has been found in bulk heterojunction poly(3-hexylthiophene):[6,6]-phenyl-C-61-butyric acid methyl ester (P3HT:PCBM) organic photovoltaic (OPV) devices. Atomic force photovoltaic microscopy (AFPM) was used to scan arrays of 2 ?m diameter OPV devices with varied indium tin oxide (ITO) surface treatments. The standard deviation of the average photocurrent was found to be 11.4% for devices fabricated on untreated ITO, 8.6% for devices with a poly(3,4-ethylenedioxythiophene):poly(styrene sulfonate) (PEDOT:PSS) interlayer, and 6.7% for devices with an HCl-treated ITO surface. These results suggest that spatial variations in the structure and electronic properties of the anode surface degrade the overall performance of OPVs including reductions in short circuit current by up to 20%, thus highlighting the importance of surface treatments that improve the homogeneity of ITO.

REPORT DOCUMENTATION PAGE (SF298)
(Continuation Sheet)

Continuation for Block 13

ARO Report Number 48138.19-CH-PCS
Influence of Indium Tin Oxide Surface Treatmen ...

Block 13: Supplementary Note

Approved for public release; distribution is unlimited.

THE JOURNAL OF PHYSICAL CHEMISTRY C

ARTICLE

pubs.acs.org/JPCC

Influence of Indium Tin Oxide Surface Treatment on Spatially Localized Photocurrent Variations in Bulk Heterojunction Organic Photovoltaic Devices

Benjamin J. Leever,[†,‡] Ian P. Murray,[‡] Michael F. Durstock,[*,†] Tobin J. Marks,[*,‡,§] and Mark C. Hersam[*,‡,§]

[†]Air Force Research Laboratory, 2941 Hobson Way, Wright-Patterson AFB, Ohio 45433-7750, United States

[‡]Department of Materials Science and Engineering, the Materials Research Center, and the Argonne Northwestern Solar Energy Research Institute, Northwestern University, 2220 Campus Drive, Evanston, Illinois 60208-3108, United States

[§]Department of Chemistry, the Materials Research Center, and the Argonne Northwestern Solar Energy Research Institute, Northwestern University, 2145 Sheridan Road, Evanston, Illinois 60208-3113, United States

Supporting Information

ABSTRACT: A correlation between anode surface treatment and spatially localized photocurrent variations has been found in bulk heterojunction poly(3-hexylthiophene):[6,6]-phenyl-C-61-butyric acid methyl ester (P3HT:PCBM) organic photovoltaic (OPV) devices. Atomic force photovoltaic microscopy was used to scan arrays of 2 μm diameter OPV devices with varied indium tin oxide (ITO) surface treatments. The standard deviation of the average photocurrent was found to be 11.4% for devices fabricated on untreated ITO, 8.6% for devices with a poly(3,4-ethylenedioxythiophene):poly(styrene sulfonate) (PEDOT:PSS) interlayer, and 6.7% for devices with a HCl-treated ITO surface. These results suggest that spatial variations in the structure and electronic properties of the anode surface degrade the overall performance of OPVs, including reductions in short-circuit current by up to 20%, thus highlighting the importance of surface treatments that improve the homogeneity of ITO.

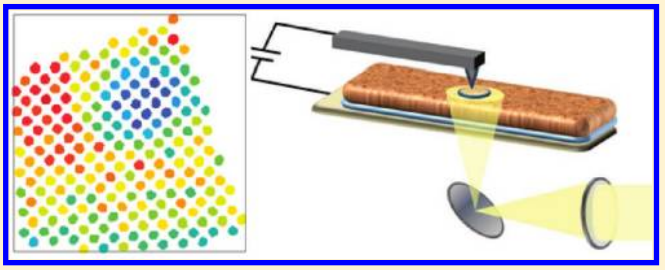

INTRODUCTION

The architecture of organic photovoltaic (OPV) devices is dominated by the bulk heterojunction (BHJ) scheme of an interpenetrating phase-separated network of an electron-donating material (such as the conjugated polymer P3HT) and an electron-accepting material (typically a fullerene). Since the BHJ design was first demonstrated,[1,2] considerable effort has focused on elucidating the nature of the resulting morphology, including its relationship with processing parameters and its impact on device operation. The morphology in BHJ OPV devices has been previously characterized by electron microscopy and tomography,[3−5] spectroscopic ellipsometry,[6] and X-ray diffraction.[7,8] In addition, scanning probe methods[9−12] have revealed nanometer-scale information about the morphology of these films while concurrently offering the additional capability of mapping electronic properties of the active layer. This work has generally pointed toward an optimal morphology consisting of crystalline P3HT nanowires (∼10−20 nm diameter) surrounded by a PCBM-rich matrix. These studies have also shown that the choice of solvent and annealing conditions can profoundly impact phase separation, with optimized devices exhibiting an ∼5% photoconversion efficiency.[7,13]

A second area of intense focus in OPV devices has been the anode, which is typically indium tin oxide (ITO) with a sheet resistance of 10−20 Ω/sq at an optical transparency of 90%. Properties, such as surface energy, work function, and conductive uniformity, have been modified by a variety of methods, including solvent cleaning,[14] exposure to UV-ozone or oxygen plasma,[15,16] and submersion in acids and bases.[17−19] Similarly, the ITO work function has been tailored through the deposition of self-assembled monolayers (SAMs) with $-CH_3$, $-NH_2$, and $-CF_3$ terminal groups,[20] and a series of phosphonic acid SAMs has been shown to allow the work function to be tuned while the surface energy is held constant.[21] More often, though, the anode surface is modified by a film of PEDOT:PSS, which is an acidic aqueous dispersion of poly(3,4-ethylenedioxythiophene) and poly(styrene sulfonate). Although the role of PEDOT:PSS in device operation is not fully understood, it is generally considered a hole-transport layer that serves to increase the anode work function, block electron transport, planarize the anode surface, and modify its surface energy.[22,23] Because of its acidic nature, however, PEDOT:PSS has been shown to create an unstable interface with the underlying ITO anode, with Rutherford backscattering (RBS)[24] and X-ray photoelectron spectroscopy (XPS) studies showing that ITO diffuses into the PEDOT:PSS film.[25] This effect has been shown to limit device lifetime,[24,26]

Received: October 4, 2011
Published: October 10, 2011

and separate work has additionally shown that PEDOT:PSS has a limited electron-blocking capability.[27] For these reasons, recent efforts have focused on identifying alternative interfacial layers, such as p-type NiO,[28,29] the polymer blend $TPDSi_2$:TFB,[30] and V_2O_5.[31]

Although previous studies have reported a correlation between anode surface energy and morphology in the BHJ layer,[6,20] the impact of interfacial modifications on photocurrent homogeneity in the BHJ layer has not been established. Scanning probe studies have shown, however, that spatially localized photocurrent variations occur in the active layer at length scales that are orders of magnitude larger than the known length scales of donor−acceptor phase separation.[9,32] Herein, we utilize atomic force photovoltaic microscopy (AFPM) to probe the influence of electrical inhomogeneities in the anode surface on photocurrent variations in the BHJ layer. In particular, we have performed AFPM on arrays of 2 μm diameter OPV devices fabricated with different anode surface treatments, including a haloacid etch and the deposition of a PEDOT:PSS interlayer. By illuminating these devices with solar simulated light and measuring their photocurrent over large scan areas, a quantitative correlation is established between the electrical heterogeneity in the anode surface and the standard deviation of the photocurrent in the BHJ layer. These results demonstrate the importance of anode uniformity in the overall performance of OPVs, thus motivating future efforts to develop improved ITO surface treatments and alternative interlayer materials.

EXPERIMENTAL METHODS

Device Preparation. ITO-coated glass (~10 Ω/sq) was purchased from Delta Technologies and cut to 12 mm × 25 mm substrates. The substrates were subsequently cleaned by sonicating for 20 min each in dilute Alconox aqueous detergent, deionized water, 2-propanol, methanol, and acetone and then blown dry with N_2. For devices with a PEDOT:PSS interlayer, the ITO substrates were cleaned in a UV-ozone chamber (Jetlight Co., model 42) for 20 min and then immediately spin-coated for 45 s at 3500 rpm with Clevios PH (H.C. Stark) that had been passed through a 0.45 μm PVDF 13 mm syringe filter (Millex-GV). The Clevios PH was stored in a refrigerator and allowed to warm to room temperature before use. To remove all water from the cast PEDOT:PSS films, the substrates were then annealed in air on a hot plate at 140 °C for 15 min. The resulting film was determined by surface profilometry (KLA Tencor P15 Stylus Profiler) to be 45 ± 3 nm thick. For devices with HCl-treated ITO, the solvent-cleaned substrates were sonicated in 0.30 M HCl for 20 min, thoroughly rinsed with deionized water, blown dry with N_2, and UV-ozone cleaned as described previously.[19] For devices with an untreated ITO surface, the substrates were cleaned by the solvent and UV-ozone treatments only. In each case, the substrates were transferred immediately after surface preparation to a N_2 glovebox (<1 ppm O_2).

The solution for the P3HT:PCBM (1:1) photoactive layer was prepared by dissolving P3HT (98% regioregular, Rieke Metals) and PCBM (>99.95%, American Dye Source) at a concentration of 18 mg/mL in 1,2-dichlorobenzene (Drisolv) that had been distilled and stored under N_2. The solution was prepared in a 10 mL N_2-purged Schlenk flask and stirred on a hot plate at 60 °C in the dark for 1 h. The P3HT:PCBM solution was then sonicated in the dark for 1 h at 50 °C and immediately loaded into a N_2 glovebox. In the glovebox, the active layer solution was passed through a 0.22 μm PTFE 13 mm syringe filter (Millex-FH) and then spin-coated onto each of the substrates (untreated, HCl-treated, and PEDOT:PSS-coated) at 550 rpm for 60 s, followed by 2000 rpm for 1 s, to give a film thickness of 200−220 nm. Although these films are typically solvent-annealed by drying in a Petri dish,[13] the films in this case were dried uncovered to reduce the surface roughness. After drying for ~5 min, the films were annealed on a hot plate at 120 °C for 10 min.

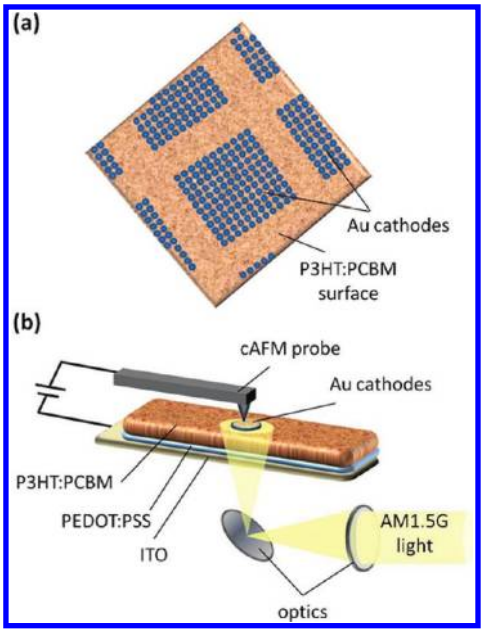

Figure 1. (a) Schematic depiction of the 90 μm × 90 μm arrays of 2 μm diameter Au cathodes evaporated through holey carbon shadow masks. (b) Schematic of the experimental setup for AFPM.

To create an array of microscopic cathodes on the P3HT:PCBM surface, a 200 mesh copper transmission electron microscopy (TEM) grid covered with a holey carbon film (Quantifoil Q225-CR4) was used as a shadow mask. The holes in the holey carbon film have a 2 μm diameter and a 6 μm period. Using a deposition system within the N_2 glovebox, electrodes were deposited by thermally evaporating gold foil (99.95%, Alfa Aesar) at a chamber pressure of ~5×10^{-6} Torr and a rate of 0.3 Å/s to a thickness of 50 nm. The resulting pattern created on the P3HT:PCBM surface consists of regularly spaced 90 μm × 90 μm arrays of 2 μm diameter gold cathodes and is shown in Figure 1a. Gold was selected as the cathode material because alternative metals were found to oxidize under the scanning conditions described below. To verify the photovoltaic response of this architecture, an $I-V$ curve was recorded for a macroscopic (~5 mm^2) device (see Figure S1, Supporting Information). It should be noted that Au has been shown to significantly reduce V_{oc} compared to Al and that the Au deposition conditions likely degrade the active layer/cathode interface and reduce the fill factor.[33−35]

Device Characterization. The microscopic solar cells were characterized via AFPM.[32] To contact the ITO anode, the organic layers were removed from the edge of the substrate with a solvent-soaked cotton swab, and a copper wire was affixed to the ITO with silver paint. The substrate (device-side up) was then attached to an optics stage (weighing less than 5 g), which rests on the piezoelectric scanner of a ThermoMicroscopes CP Research AFM. The devices were illuminated through the glass side of the substrate by a Newport Oriel 96000 solar light simulator equipped with an AM 1.5G filter and a liquid light

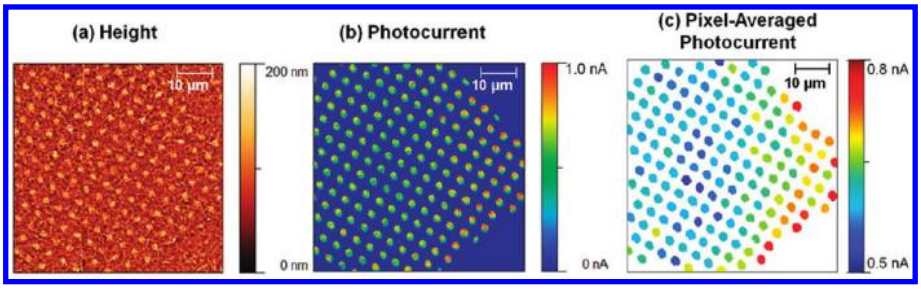

Figure 2. AFPM images for devices with a PEDOT:PSS interlayer: (a) height, (b) photocurrent, and (c) pixel-averaged photocurrent. Note that the absolute value of the photocurrent is depicted.

guide (Newport Oriel 77638). Optics at the end of the liquid light guide collimate the light into a small beam about the same size as the plano-convex lens in the optics stage. The lens then focuses the light onto a convex mirror, which reflects the light onto the substrate, thus illuminating the devices. The intensity of the solar-simulated light is 7 suns (700 mW/cm^2), which increases the signal-to-noise ratio of the resulting photocurrent compared to 1 sun illumination.

The gold cathodes were addressed by scanning them under ambient conditions in contact mode with Nanosensors boron-doped, diamond-coated cAFM probes (model CDT-FMR). The probes have an average force constant of 2.8 N/m, and forces from 15 to 60 nN were applied to the probes as they were raster scanned across the array of devices. During scanning, a dc bias can be applied through the wire attached to the ITO, and the resulting photocurrent that passes through the grounded cAFM probe is measured with a DL Instruments current preamplifier. The experimental setup is depicted in Figure 1b.

RESULTS AND DISCUSSION

Figure 2 depicts the height and photocurrent micrographs simultaneously collected during an AFPM scan as well as a "pixel-averaged" photocurrent map. In an effort to minimize confusion, all current maps indicate the absolute value of the current. Although the sample−probe contact is improved by scanning metal cathodes rather than the BHJ surface directly; some variability remains due to the roughness of the Au pads. Therefore, to minimize the effect of this imaging artifact, we have averaged the photocurrent over each device. In particular, the 70 μm × 70 μm pixel-averaged scan in Figure 2 demonstrates significant variability among devices with a PEDOT:PSS interlayer at the short-circuit current condition. The photocurrent ranges from approximately 0.5 to 0.8 nA for these ∼3 μm^2 devices. Because the resolution of AFPM is limited by the size of the metal cathodes, these smaller devices improve the AFPM resolution by over an order of magnitude compared to the ∼56 μm^2 devices in our previous report[32] and reveal a device-to-device variability (∼50%) that is twice as large as our observation for the larger devices.

In previous reports, scanning probe investigations have analyzed photocurrent variability in BHJ OPV films by both directly contacting the BHJ surface with the cAFM probe[9,36,37] and by contacting microscopic, fully functioning devices,[32,36] as reported here. Although quantitative analysis is difficult when the probe directly contacts the BHJ surface (due to the variable contact area), the topography and photocurrent have been simultaneously recorded for both poly[2-methoxy-5-(3′,7′-dimethyloctyl-oxy)-1,4-phenylene vinylene]:(6,6)-phenyl-C-61-butyric acid methyl ester (MDMO-PPV:PCBM)[9] and P3HT:PCBM BHJ[36,37] films. Photocurrent scans of MDMO-PPV:PCBM films exhibited a clear correlation with the apparent morphology in the topography map. However, analysis of the P3HT:PCBM film has proven more complex, potentially because of the smaller phase-separated domains in this case. For P3HT:PCBM devices, photocurrent variability spanning 1−2 orders of magnitude has been observed in scan areas < 5 μm × 5 μm at short-circuit conditions. In one report, the regions of high photocurrent were attributed to PCBM-rich domains in the film surface,[36] whereas another report attributed the areas of increased photocurrent to spatially localized regions of optimal morphology.[37]

When operating microscopic devices have been probed, the variability in photocurrent has been found to decrease with increasing device size. In our work, we have seen variability of ∼50% in 3 μm^2 devices, as shown in Figure 2, as well as variability of ∼25% at a 56 μm^2 scale.[32] Similar observations have been made for smaller devices, with 0.01 μm^2 devices having photocurrents ranging over a factor of 10, and the photocurrent for devices 0.03−0.06 μm^2 in size varying by over a factor of 2. While increasing the device size would be expected to average out photocurrent fluctuations, this variability clearly persists at length scales that are orders of magnitude larger than those associated with phase-separated domains occurring in these films.

Beyond the active layer morphology, it has also been suggested that the surface adjacent to the BHJ film (either the ITO or an interfacial layer) could be a source of inhomogeneity in these devices.[9,19,29,30] Scanning probe microscopy and X-ray photoelectron spectroscopy (XPS) have shown conductive heterogeneity in the ITO surface.[38,39] These "hot spots" (areas of increased conductance) and "dead spots" (areas of reduced conductance) have been attributed to variations in the ITO surface chemistry as well as to carbon contamination. Chemical variations in the ITO surface have been found to include stoichiometric regions of In_2O_3 and SnO_2, the presence of hydrolyzed oxides and oxyhydroxides, and oxygen defect sites.[40] Similarly, scanning tunneling microscopy (STM) and cAFM analysis of PEDOT:PSS films have shown significant variability in the surface conductance, in this case, due to PEDOT- and PSS-rich regions within the film.[41,42] In addition, improved performance has been demonstrated in devices fabricated with anode surface treatments or interfacial layers known to improve the conductive uniformity of the anode surface, further suggesting a link between the variability in the anode and the performance of the BHJ layer.

To determine the impact of conductance variations in the anode surface on spatially localized photocurrent variations within the P3HT:PCBM layer, numerous AFPM scans were performed

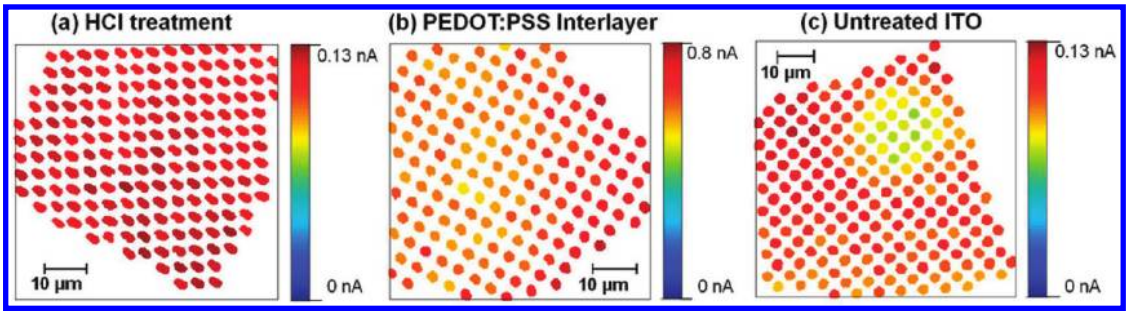

Figure 3. Pixel-averaged AFPM photocurrent maps of (a) devices with HCl-treated ITO, (b) devices with a PEDOT:PSS interlayer, and (c) devices with untreated ITO. Note that the absolute value of the photocurrent is depicted.

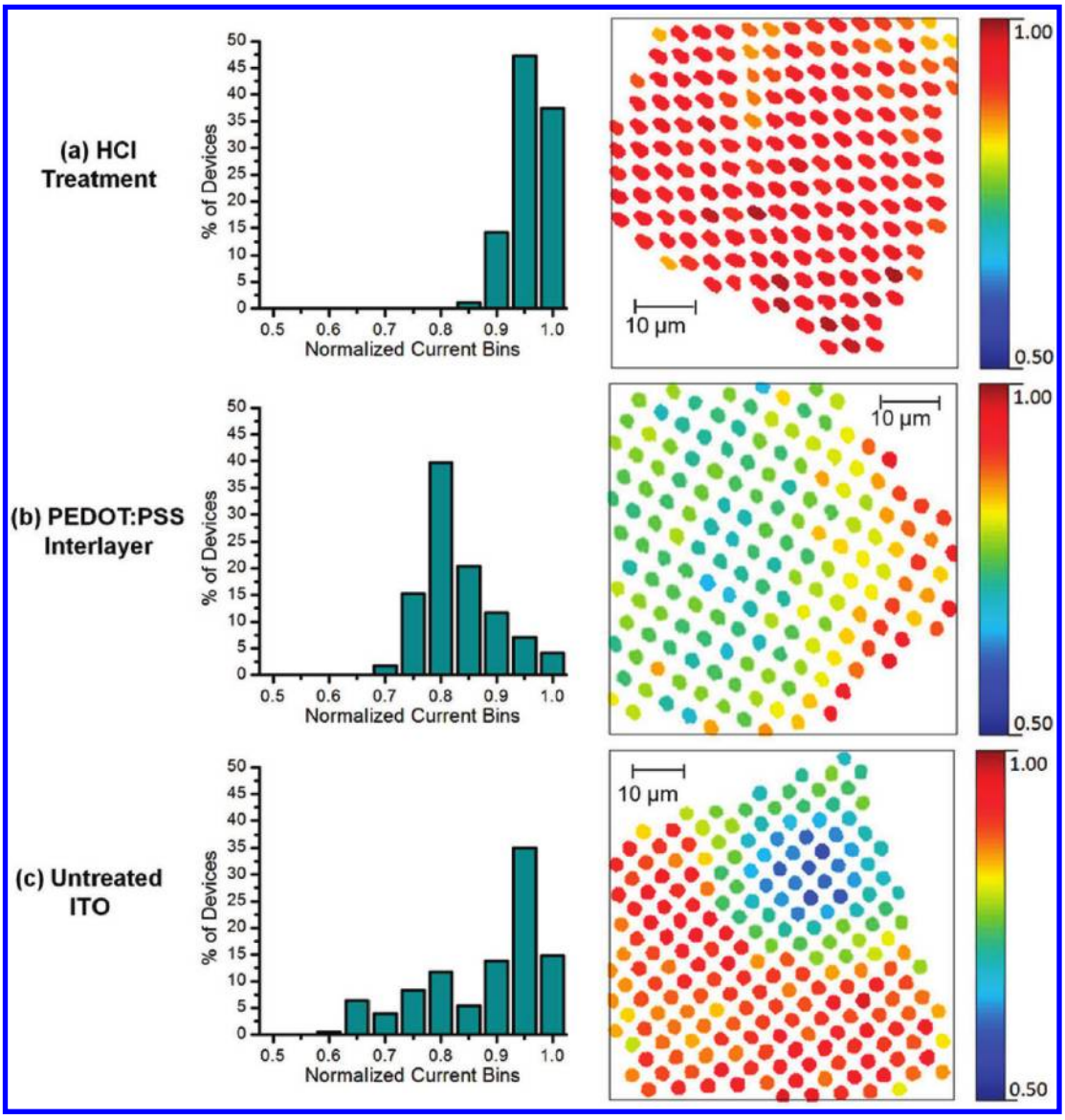

Figure 4. Histograms and normalized current maps for individual AFPM scans of devices with (a) HCl-treated ITO, (b) PEDOT:PSS interlayer, and (c) no interfacial treatment. Note that the absolute value of the photocurrent is depicted.

on a series of devices with varied anode surfaces. BHJ devices (3 μm^2) were fabricated on the following: (1) substrates with ITO that had been solvent-cleaned and UVO-cleaned only, (2) substrates with an HCl-treated ITO surface, and (3) substrates with a PEDOT:PSS interlayer. Figure 3 depicts representative pixel-averaged photocurrent maps for these device configurations.

dx.doi.org/10.1021/jp209570h |J. Phys. Chem. C 2011, 115, 22688–22694

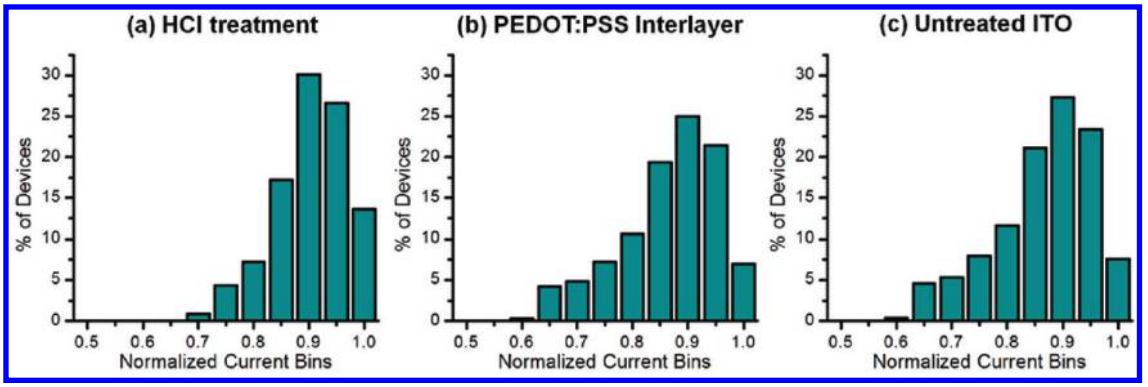

Figure 5. Multiscan AFPM histograms for devices with (a) HCl-treated ITO, (b) PEDOT:PSS interlayer, and (c) untreated ITO. Note that the photocurrent was normalized for each scan. Normalized photocurrent values were then combined for each device type and binned.

The photocurrent map shows significantly less spatial variation in the devices with an HCl-treated anode (Figure 3a) than in devices with either a PEDOT:PSS interlayer (Figure 3b) or an untreated anode (Figure 3c).

To better quantify the variability in individual current maps, histograms were produced from the current maps in Figure 3. To create the histograms, the average photocurrent was calculated for each device in an individual current map. Note that partial devices from the scan edges were excluded. The average photocurrent of each device was then normalized to the maximum photocurrent in the scan and sorted into bins with a width of 5%. The percentage of devices in each bin was then plotted from 0.5 to 1.0 (the fraction of the maximum average photocurrent). Both the histograms and the normalized current maps are shown in Figure 4. For these data sets, a clear increase in device-to-device variability is observed from devices with HCl-treated ITO (top) as compared to devices with a PEDOT:PSS interlayer (middle) or to devices with no anode treatment (bottom).

In addition to determining the variability in individual scans, the average variability (over several scans) was also quantified for each device configuration, thus allowing for better overall statistics. For the histograms depicted in Figure 5, the photocurrent was normalized for each scan, and normalized photocurrent values were then combined for each device type and binned. While nearly all the devices with the HCl treatment have a photocurrent within ~25% of the maximum, the photocurrent ranges increase to about 35% and 40% for devices with PEDOT:PSS and untreated ITO, respectively. Overall, devices treated with HCl had a standard deviation that was 6.7% of the average photocurrent, whereas the standard deviation increased to 8.6% and 11.4% of the average photocurrent for devices with a PEDOT:PSS interlayer and no anode treatment, respectively.

Our AFPM results demonstrate a strong correlation between anode surface treatment and spatial variations in the photocurrent, implying that the effects of "hot spots" and "dead spots" are transferred through the active layer film. In previous reports,[19,29] we have shown the spatial extent of these effects and the impact of ITO surface treatments on surface conductance at smaller length scales. To illustrate the heterogeneity in surface conductance at the length scales studied here, cAFM images of untreated ITO and HCl-etched ITO are included (Figure S2, Supporting Information). In addition, while we have previously shown at a macroscopic scale that interfacial treatments increase the open-circuit voltage (V_{oc}) and shunt resistance while decreasing the series resistance,[19] this work establishes that the conductive uniformity of the anode surface could be tailored to modify the photocurrent. This result contrasts with earlier work that attributed variability at a smaller length scale to the phase-segregated nature of the BHJ film.[36,37] Although variability related to the film nanostructure will inevitably be present, our observations at these larger length scales provide a specific opportunity for performance enhancement, that is, the use of anode surface treatments or interfacial layers that improve conductive uniformity. Relating these results to device performance, the macroscopic device (with untreated ITO) in Figure S2 (Supporting Information) exhibited a J_{sc} of 4.7 mA/cm^2. Assuming that this device exhibited the same photocurrent variability depicted in Figure 5c, the J_{sc} could be improved ~20% to 5.9 mA/cm^2 if the entire film uniformly exhibited the observed maximum localized photocurrent.

AFPM was also employed to study devices at a variety of applied DC biases. Figure 6 depicts histograms and normalized current maps for a single array of devices fabricated on untreated ITO and scanned at three different biases. Although the average photocurrent is nearly doubled by changing the applied bias from 0.0 V to −200 mV, the standard deviation is ~11.5% of the average photocurrent in both cases. On the other hand, when a larger positive bias is applied, the standard deviation is reduced. In the case of Figure 6c, where a +450 mV bias is applied, the standard deviation was determined to be ~7.5% of the average photocurrent. This result is consistent with $I-V$ curves on microscopic devices, which show more uniform current near V_{oc} and extending into the first quadrant. This behavior suggests that the impact of photocurrent variability could potentially be mitigated by operating the solar cell at higher biases.

Although this work focused on BHJ OPV devices, AFPM is a general technique that can be extended to numerous other thin film photovoltaic (PV) technologies for similar investigations of photocurrent variability. Thin film PV devices typically include a transparent conducting oxide, such as ITO,[43−45] and thus may also exhibit similar spatially localized current variations (and an associated suboptimal performance) due to variability in the ITO surface conductance. In addition, AFPM has the potential to reveal photocurrent variations related to the grain structure in thin film PV devices, such as polycrystalline silicon,[46] CdTe/CdS,[47] and Cu(InGa)Se$_2$[48] (CIGS), or to the nanoparticles or patterned back electrode in plasmonic

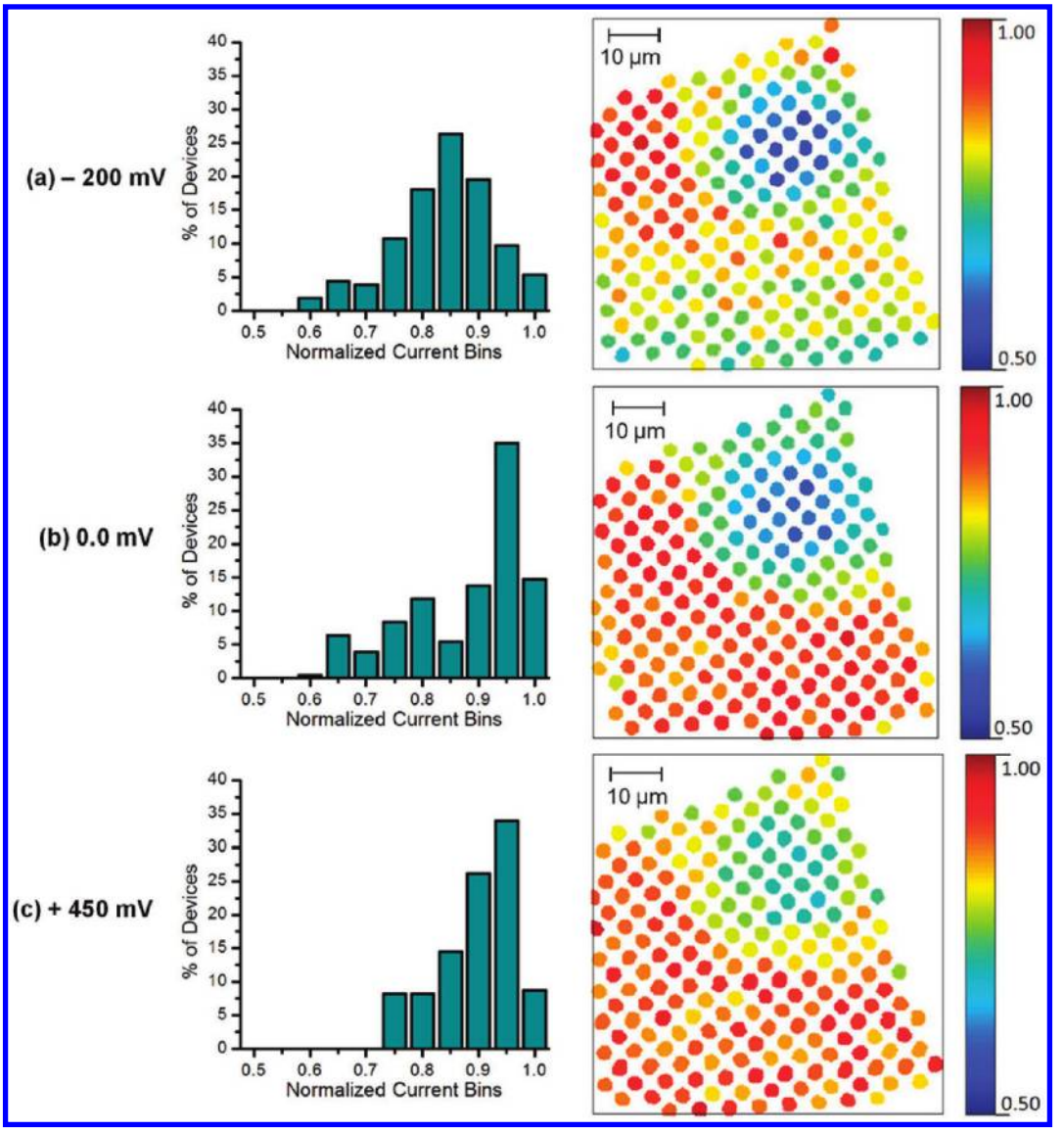

Figure 6. AFPM histograms and normalized current maps for a single array of devices on untreated ITO scanned at three different applied biases: (a) −200, (b) 0.0, and (c) +450 mV. Note that the absolute value of the photocurrent is depicted.

solar cells.[49] New insights in these devices could provide additional routes for performance enhancements or serve as a quality control measure in device production.

CONCLUSIONS

By fabricating 2 μm diameter OPV devices on ITO with different surface treatments, we have used AFPM to establish a quantitative correlation between the conductive uniformity of the anode surface and photocurrent variations in the P3HT:PCBM film. Devices tested on ITO coated with PEDOT:PSS or treated with HCl are shown to significantly reduce photocurrent variation at the micrometer scale compared to devices fabricated on untreated ITO, providing a promising avenue for performance enhancements in these devices. Interfacial layers or treatments that optimize anode conductive uniformity show promise for increasing J_{sc} by up to 20% as compared to a device with untreated ITO. We have also shown that the device-to-device variation is reduced at forward biases, suggesting an additional opportunity for mitigating the variability in photocurrent. These results demonstrate that conductive uniformity is an important consideration for new OPV interfacial materials or related anode surface treatments and that additional insight can be gained by extending AFPM analysis to other thin film PV technologies.

ASSOCIATED CONTENT

Supporting Information. Macroscopic device $I-V$ curve and anode cAFM images. This material is available free of charge via the Internet at http://pubs.acs.org.

AUTHOR INFORMATION

Corresponding Author

*E-mail: m-hersam@northwestern.edu (M.C.H.), t-marks@northwestern.edu (T.J.M.), Michael.Durstock@wpafb.af.mil (M.F.D.).

■ ACKNOWLEDGMENT

This work was supported by the ANSER Energy Frontier Research Center (funded by the Department of Energy, grant DE-SC0001059), the Army Research Office (ARO W911NF-05-1-0177), the Air Force Office of Scientific Research, and the Air Force Research Laboratory Materials & Manufacturing Directorate.

■ REFERENCES

(1) Yu, G.; Heeger, A. J. *J. Appl. Phys.* **1995**, *78*, 4510–4515.
(2) Halls, J. J. M.; Walsh, C. A.; Greenham, N. C.; Marseglia, E. A.; Friend, R. H.; Moratti, S. C.; Holmes, A. B. *Nature* **1995**, *376*, 498–500.
(3) Yang, X.; Loos, J.; Veenstra, S. C.; Verhees, W. J. H.; Wienk, M. M.; Kroon, J. M.; Michels, M. A. J.; Janssen, R. A. *J. Nano Lett.* **2005**, *5*, 579–583.
(4) van Bavel, S. S.; Sourty, E.; de With, G.; Loos, J. *Nano Lett.* **2008**, *9*, 507–513.
(5) van Bavel, S. S.; Bärenklau, M.; de With, G.; Hoppe, H.; Loos, J. *Adv. Funct. Mater.* **2010**, *20*, 1458–1463.
(6) Campoy-Quiles, M.; Ferenczi, T.; Agostinelli, T.; Etchegoin, P. G.; Kim, Y.; Anthopoulos, T. D.; Stavrinou, P. N.; Bradley, D. D. C.; Nelson, J. *Nat. Mater.* **2008**, *7*, 158–164.
(7) Ma, W.; Yang, C.; Gong, X.; Lee, K.; Heeger, A. *Adv. Funct. Mater.* **2005**, *15*, 1617–1622.
(8) Kim, Y.; Cook, S.; Tuladhar, S. M.; Choulis, S. A.; Nelson, J.; Durrant, J. R.; Bradley, D. D. C.; Giles, M.; McCulloch, I.; Ha, C.-S.; Ree, M. *Nat. Mater.* **2006**, *5*, 197–203.
(9) Coffey, D. C.; Reid, O. G.; Rodovsky, D. B.; Bartholomew, G. P.; Ginger, D. S. *Nano Lett.* **2007**, *7*, 738–744.
(10) Douheret, O.; Lutsen, L.; Swinnen, A.; Breselge, M.; Vandewal, K.; Goris, L.; Manca, J. *Appl. Phys. Lett.* **2006**, *89*, 032107.
(11) McNeill, C. R.; Frohne, H.; Holdsworth, J. L.; Furst, J. E.; King, B. V.; Dastoor, P. C. *Nano Lett.* **2004**, *4*, 219–223.
(12) Palermo, V.; Palma, M.; Samorì, P. *Adv. Mater.* **2006**, *18*, 145–164.
(13) Li, G.; Shrotriya, V.; Huang, J. S.; Yao, Y.; Moriarty, T.; Emery, K.; Yang, Y. *Nat. Mater.* **2005**, *4*, 864–868.
(14) Sugiyama, K.; Ishii, H.; Ouchi, Y.; Seki, K. *J. Appl. Phys.* **2000**, *87*, 295–298.
(15) Halls, J. J. M.; Walsh, C. A.; Greenham, N. C.; Marseglia, E. A.; Friend, R. H.; Moratti, S. C.; Holmes, A. B. *Nature.* **1995**, *376*, 498–500.
(16) Chkoda, L.; Heske, C.; Sokolowski, M.; Umbach, E.; Steuber, F.; Staudigel, J.; Stößel, M.; Simmerer, J. *Synth. Met.* **2000**, *111−112*, 315–319.
(17) Nuesch, F.; Rothberg, L. J.; Forsythe, E. W.; Toan Le, Q.; Gao, Y. *Appl. Phys. Lett.* **1999**, *74*, 880–882.
(18) Brumbach, M.; Veneman, P. A.; Marrikar, F. S.; Schulmeyer, T.; Simmonds, A.; Xia, W.; Lee, P.; Armstrong, N. R. *Langmuir* **2007**, *23*, 11089–11099.
(19) Irwin, M. D.; Liu, J.; Leever, B. J.; Servaites, J. D.; Hersam, M. C.; Durstock, M. F.; Marks, T. J. *Langmuir* **2010**, *26*, 2584–2591.
(20) Kim, J. S.; Park, J. H.; Lee, J. H.; Jo, J.; Kim, D.-Y.; Cho, K. *Appl. Phys. Lett.* **2007**, *91*, 112111.
(21) Hotchkiss, P. J.; Li, H.; Paramonov, P. B.; Paniagua, S. A.; Jones, S. C.; Armstrong, N. R.; Brédas, J. L.; Marder, S. R. *Adv. Mater.* **2009**, *21*, 4496–4501.
(22) Cao, Y.; Yu, G.; Zhang, C.; Menon, R.; Heeger, A. *J. Synth. Met.* **1997**, *87*, 171–174.
(23) Huang, J.; Miller, P. F.; de Mello, J. C.; de Mello, A. J.; Bradley, D. D. C. *Synth. Met.* **2003**, *139*, 569–572.
(24) Kim, Y.-H.; Lee, S.-H.; Noh, J.; Han, S.-H. *Thin Solid Films* **2006**, *510*, 305–310.
(25) Chen, L.-M.; Xu, Z.; Hong, Z.; Yang, Y. *J. Mater. Chem.* **2010**, *20*, 2575–2598.
(26) de Jong, M. P.; van Ijzendoorn, L. J.; de Voigt, M. J. A. *Appl. Phys. Lett.* **2000**, *77*, 2255–2257.
(27) Yan, H.; Lee, P.; Armstrong, N. R.; Graham, A.; Evmenenko, G. A.; Dutta, P.; Marks, T. J. *J. Am. Chem. Soc.* **2005**, *127*, 3172–3183.
(28) Irwin, M. D.; Buchholz, D. B.; Hains, A. W.; Chang, R. P. H.; Marks, T. J. *Proc. Natl. Acad. Sci. U.S.A.* **2008**, *105*, 2783–2787.
(29) Irwin, M. D.; Servaites, J. D.; Buchholz, D. B.; Leever, B. J.; Liu, J.; Emery, J. D.; Zhang, M.; Song, J.-H.; Durstock, M. F.; Freeman, A. J.; Bedzyk, M. J.; Hersam, M. C.; Chang, R. P. H.; Ratner, M. A.; Marks, T. *J. Chem. Mater.* **2011**, *23*, 2218–2226.
(30) Hains, A. W.; Marks, T. *J. Appl. Phys. Lett.* **2008**, *92*, 023504.
(31) Shrotriya, V.; Li, G.; Yao, Y.; Chu, C.-W.; Yang, Y. *Appl. Phys. Lett.* **2006**, *88*, 073508.
(32) Leever, B. J.; Durstock, M. F.; Irwin, M. D.; Hains, A. W.; Marks, T. J.; Pingree, L. S. C.; Hersam, M. C. *Appl. Phys. Lett.* **2008**, *92*, 013302.
(33) Ramsdale, C.; Barker, J.; Arias, A.; MacKenzie, J.; Friend, R.; Greenham, N. *J. Appl. Phys.* **2002**, *92*, 4266–4270.
(34) Mihailetchi, V.; Blom, P.; Hummelen, J.; Rispens, M. *J. Appl. Phys.* **2003**, *94*, 6849–6854.
(35) Glatthaar, M.; Riede, M.; Keegan, N.; Sylvester-Hvid, K.; Zimmermann, B.; Niggemann, M.; Hinsch, A.; Gombert, A. *Sol. Energy Mater. Sol. Cells* **2007**, *91*, 390–393.
(36) Hamadani, B. H.; Jung, S.; Haney, P. M.; Richter, L. J.; Zhitenev, N. B. *Nano Lett.* **2010**, *10*, 1611–1617.
(37) Pingree, L. S. C.; Reid, O. G.; Ginger, D. S. *Nano Lett.* **2009**, *9*, 2946–2952.
(38) Liau, Y. H.; Scherer, N. F.; Rhodes, K. *J. Phys. Chem. B* **2001**, *105*, 3282–3288.
(39) Lin, H. N.; Chen, S. H.; Perng, G. Y.; Chen, S. A. *J. Appl. Phys.* **2001**, *89*, 3976–3979.
(40) Donley, C.; Dunphy, D.; Paine, D.; Carter, C.; Nebesny, K.; Lee, P.; Alloway, D.; Armstrong, N. R. *Langmuir* **2001**, *18*, 450–457.
(41) Kemerink, M.; Timpanaro, S.; de Kok, M. M.; Meulenkamp, E. A.; Touwslager, F. J. *J. Phys. Chem. B* **2004**, *108*, 18820–18825.
(42) Nardes, A.; Kemerink, M.; Janssen, R.; Bastiaansen, J.; Kiggen, N.; Langeveld, B.; van Breemen, A.; de Kok, M. *Adv. Mater.* **2007**, *19*, 1196–1200.
(43) Aberle, A. G. *Thin Solid Films* **2009**, *517*, 4706–4710.
(44) Chopra, K. L.; Paulson, P. D.; Dutta, V. *Prog. Photovoltaics* **2004**, *12*, 69–92.
(45) Ginley, D.; Green, M. A.; Collins, R. *MRS Bull.* **2008**, *33*, 355–364.
(46) Van Gestel, D.; Romero, M. J.; Gordon, I.; Carnel, L.; D'Haen, J.; Beaucarne, G.; Al-Jassim, M.; Poortmans, J. *Appl. Phys. Lett.* **2007**, *90*, 092103.
(47) Durose, K.; Cousins, M. A.; Boyle, D. S.; Beier, J.; Bonnet, D. *Thin Solid Films* **2002**, *403−404*, 396–404.
(48) Rau, U.; Taretto, K.; Siebentritt, S. *Appl. Phys. A: Mater. Sci. Process.* **2009**, *96*, 221–234.
(49) Atwater, H. A.; Polman, A. *Nat. Mater.* **2010**, *9*, 205–213.